On the Impact of Proprioception in EEG Representations and Decoding during Human-Hand Exoskeleton Interaction

Qiang Sun, Eva Calvo Merino, Liuyin Yang, Axel Faes, and Marc M. Van Hulle

Abstract—Controlling a hand exoskeleton based on electroencephalogram (EEG)-based brain-computer interfacing (BCI) holds promise for human motor augmentation and neurorehabilitation. To achieve natural control, a critical step is to understand the impact of proprioception provided by the exoskeleton during interaction. In this study, we aim to approach the goal by quantifying EEG representations and BCI performance. We monitored 25 healthy subjects' full-scalp EEG while performing different finger movement tasks with a cable-driven hand exoskeleton. Each task involves three movement modalities, i.e., imagined (IM), passive (PM), and congruent imagined and passive (IPM) finger flexion. We found that alpha (8 - 13 Hz) and beta (13 - 30 Hz) band desynchronization in the sensorimotor area was significantly stronger for PM and IPM tasks compared to IM, with no significant difference between PM and IPM. Using machine learning models, we achieved a high accuracy in classifying exoskeleton-assisted movements from the rest condition (IPM vs. REST: 0.80 ± 0.07, PM vs. REST: 0.72 ± 0.10), with the IPM modality returning the highest accuracy. However, distinguishing between IPM and PM yielded only 0.61 ± 0.09, significantly lower than the condition of intention detection without the exoskeleton (IM vs. REST: 0.73 ± 0.08). Our findings suggest that sensorimotor EEG activity can track proprioceptive feedback induced by the hand exoskeleton. While this feedback is pronounced and distinguishable, detecting motor intention during exoskeleton movement remains highly challenging. This highlights the need for advanced decoders and control strategies for the future development of continuous BCI-actuated hand exoskeletons.

Index Terms—brain-computer interfaces (BCIs), electroencephalogram (EEG), hand exoskeleton, motor intention, proprioception.

I. INTRODUCTION

Brain-computer interfaces (BCIs) build a direct connection between the human brain and effectors, bypassing the normal neuromuscular pathway [1]. A promising field for BCI systems is human motor augmentation and neurorehabilitation, where the end users can rely on a brain-actuated exoskeleton to accomplish daily activities. For practical considerations, electroencephalogram (EEG) is recommended for recording brain activities as it is non-invasive, affordable, and offers relatively high temporal and spatial resolution compared to other non-invasive recording techniques. A successful demonstration has been realized by Soekadar *et al.* [2], where an individual with impaired hand function could accomplish different daily hand tasks with an EEG-controlled exoskeleton.

Exoskeletons are widely used in neurorehabilitation to encourage the patient's engagement which in turn promotes motor recovery [3]. A BCI-controlled exoskeleton is particularly useful in this case as the patient's active motor intentions can be decoded and translated into exoskeleton commands. For patients with limited motor control functions, their intentions are conveyed through imagined movement, a type of movement that motor-disabled individuals can do by imagining a given movement without actually performing it [2], [4]. Such a closed-loop active robot-assisted mode has been shown to improve post-stroke rehabilitation outcomes [4]. In this study, we focused on BCI-actuated hand exoskeletons, as they hold promise for restoring intuitive finger control in people with hand motor impairments.

A major feature of human-exoskeleton interaction, compared to human-robotic arm or avatar interaction, is the strong proprioceptive feedback provided by the device. Once the exoskeleton is activated, the user can sense body posture and limb movements during physical interaction, leading to the excitation of the sensorimotor cortex [5]–[7]. From ongoing EEG, this excitatory activity is characterized by a power decrease or increase in particular frequency bands, termed event-related desynchronization (ERD) and event-related synchronization (ERS), respectively [8]. Specifically, robot-assisted passive movement can elicit bilaterally distributed alpha (8 - 13 Hz) and beta (13 - 30 Hz) ERD during the movement, albeit stronger on the contralateral side [5], [7]. Once the movement is terminated, ERS in the beta band occurs centrally, partially reflecting an active inhibition of the motor cortex by somatosensory afferents [9].

From a control perspective, it is pivotal to develop asynchronous and, ideally, continuous BCI, as it attributes to the autonomy of the user and provides more natural control capabilities. An asynchronous BCI system allows the user to voluntarily decide when to initiate or terminate a task. In contrast, a continuous BCI system provides ongoing, real-time outputs that continuously map the user's brain activity

to control parameters, such as movement or speed, reflecting their dynamic motor intentions. Both types of BCIs rely on real-time monitoring and decoding of the user's motor intentions. However, as the exoskeleton will produce proprioceptive afferents during interaction, the difficulty of motor intention decoding from EEG needs to be addressed. Indeed, a recent study reported that motor intention detection is more challenging during lower-limb exoskeleton interaction compared to a static case [10]. However, whether this phenomenon pertains to hand exoskeletons remains unexplored.

In this study, we designed an experimental paradigm combining a cable-driven hand exoskeleton and full-scalp EEG recordings. Our first objective is to compare the EEG representations of different movement modalities, including imagined (IM), passive (PM), and congruent imagined and passive (IPM) finger flexions, with a particular interest in comparing IPM and PM. The second objective is to assess motor intention detection performance in situations with and without exoskeleton assistance. Based on our findings, we highlight the key challenges of EEG decoding during human-hand exoskeleton interaction.

II. MATERIALS AND METHODS

A. Subjects

We recruited 25 right-handed subjects (12 males and 13 females, 24.20 ± 3.29 years old). Each subject's handedness was evaluated using the Edinburgh Handedness Inventory[1]. All subjects participated in a single-session EEG experiment. This study was approved by the Ethical Committee of the University Hospital of KU Leuven (UZ Leuven) under reference number S6254. Before the experiment, all subjects were informed about the study details and gave their written consent.

B. Experimental setup and paradigm details

The experiment was conducted in a quiet recording room. Subjects sat on a comfortable chair wearing the EEG cap and a right-hand exoskeleton, as illustrated in Fig. 1a. We configured 62 EEG active electrodes (Easycap GmbH, Germany) covering the full scalp following the 10%-System. Additional reference and ground electrodes were placed at FCz and AFz, respectively. When preparing the electrodes, we kept the impedance below 5kΩ. For EEG recording, we used the Neuroscan SynAmps RT device (Compumedics, Australia) operating at 1000 Hz sampling rate. As for the exoskeleton, we used the Gloreha Sinfonia (renamed R-TOUCH by BTL Industries). This device enables one degree-of-freedom for each finger and controls its flexion and extension by an electric actuator-driven steel cable (Fig. 1b).

The paradigm instructions were shown on the screen (View-Pixx, Canada) in front of the subjects (Fig. 1a). We designed three movement modalities, namely, IM, PM, and IPM. Each modality had three finger tasks including thumb, index, and middle-ring-little finger flexion. The timing of an exemplary
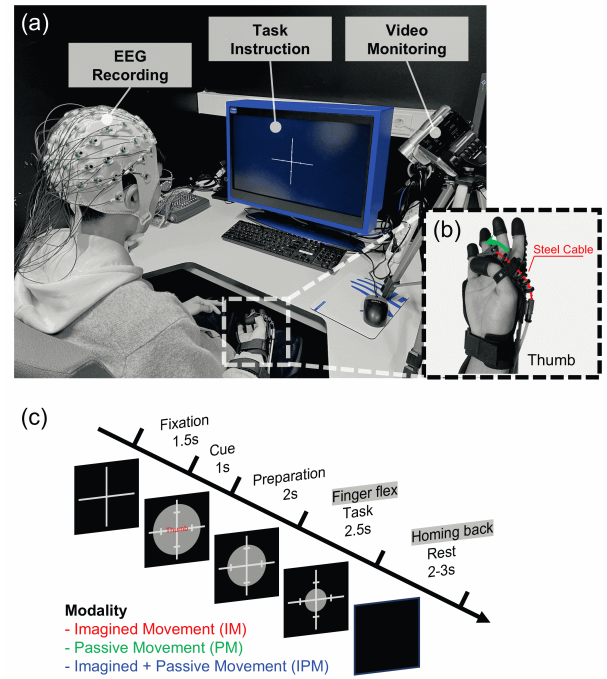
Fig. 1. Experimental paradigm. (a) Experimental setup. The subject wore a hand exoskeleton and performed the instructed tasks while the full-scalp EEG signals were recorded. (b) The exoskeleton made the thumb of the subject flex via a steel cable. (c) Timing of an exemplary imagined thumb movement trial.

imagined thumb trial is shown in Fig. 1c. At the beginning of the trial, a cross was shown on the screen for 1.5s instructing the subject to stay focused. Later, a circle and tick marks, were shown, centered on the cross, as well as a word cue indicating the finger task to be performed. Upon the disappearance of the word cue (1s later), the circle started to shrink at a constant speed. Once the circle touched the tick marks(2s later), the subject performed the finger task, either by imaging finger flexion (IM and IPM conditions) or by refraining from any mental tasks but by undergoing (and feeling) the exoskeleton movement (PM condition). After 2.5s, the subject could relax for 2-3s. There was a homing-back action from the exoskeleton in the PM and IPM conditions. For IM and IPM, we asked our subjects to perform kinesthetic imagination, i.e., imagine they were moving their right-hand fingers at the same speed as the shrinking circle. For PM, we asked our subjects to avoid any mental tasks. The exoskeleton moved the fingers at the same speed. The experiment had 30-40 rounds with each round randomizing three modalities each one comprising three randomized finger tasks. The subjects could relax between rounds and were given a form to report the trials they did wrong in the past round. All subjects practiced the paradigm prior to the real experiment. A camera monitored the behavior of each subject's right hand during the entire experiment.

C. EEG data preprocessing

Data preprocessing was done based on customized MATLAB code and scripts from the FieldTrip toolbox [11]. The recorded raw EEG data were downsampled to 250 Hz for ease

of computation after applying an antialiasing filter. Then, two notch filters were applied to remove power line noise at 50 Hz and 100 Hz. Next, we filtered the continuous signals into 0.1 - 120 Hz. The mentioned filters were all 3-order Butterworth IIR filters. Before removing eye movement artifacts, we visually inspected and removed faulty channels noted during the recording. Then, we used independent component analysis (*runica* implemention in FieldTrip) to detect vertical and horizontal eye movement-related components and removed them. Common average referencing was implemented. Finally, we imputed the excluded noisy channel EEGs based on those of neighboring electrodes.

The cleaned EEGs were segmented into 9-s epochs according to trial markers, starting from trial onset (Fig. 1c). For each epoch, we detected the noisy channels based on features: kurtosis, mean value, and variance. Specifically, a channel was detected as noisy if any of its features exceeded three times the standard deviation of the mean for all channels. The noisy channels were interpolated. We also removed bad epochs when a third of the channels had an amplitude over ±100 μV.

D. EEG representations

We looked into event-related spectrum perturbation (ERSP) of the EEG signals, which reflects the spectra power changes relative to a baseline. The group-averaged ERSP for a given finger task at channel c, frequency f, and time t is calculated as:

$$ERSP(c,f,t) = \frac{1}{S} \sum_{s=1}^{S} \frac{1}{N} \sum_{n=1}^{N} \left(F_{s,n,c}(f,t) - F_{s,n,c}^{baseline}(f) \right)$$
(1)

where S and N represent the number of subjects and the number of trials in the current task, respectively. $F_{s,n,c}$ indicates the time-frequency representation (TFR) of the c-th channel and n-th trial from subject s. We calculated the averaged power from 0.5 to 1.5s with respect to the appearance of the cross during the fixation phase (Fig. 1c) as the baseline $F_{s,n,c}^{baseline}$. The TFRs were calculated based on Short-Time Fourier Transform (STFT) with a window of 1s and overlap of 1 sample. We took the logarithm for ERSP calculation.

EEG oscillatory activities in the alpha (8 - 13 Hz) and beta (13 - 30 Hz) bands were specifically analyzed, as these rhythms are characteristic of both active and passive finger movements [6], [12]. We first visualized the topographical distribution of alpha and beta ERSP on the scalp. Then, we looked into the TFR of the representative EEG channels.

E. Decoding models

We built four binary classification models based on the Fisher Geodesic Minimal Distance to Mean (FgMDM) classifier [13]. FgMDM works in the Riemannian space and shows exceptional decoding performance in many BCI tasks [14]. In the first model, we classified IM versus the resting state (IM vs. REST), representing motor intention detection without exoskeleton movement. The second and third models classified PM versus REST and IPM versus REST, respectively, to assess

whether the exoskeleton induces distinguishable features. The final model classified IPM versus PM (IPM vs. PM), simulating a scenario to determine the presence of motor intention during exoskeleton interaction. We pooled all three finger tasks' epochs together for IM, PM, and IPM. The cleaned epochs were further bandpassed into 4 - 40 Hz. Considering the shorter displacement of thumb flexion and future online BCI applications, we opted for a 1-s data length to test decoding performance. Therefore, we extracted the first 1-second segment (time window: 4.5 – 5.5 s) from the task period for IM, PM, and IPM, respectively (Fig. 1c). For the resting state, a 1-second segment (time window: 0.5 – 1.5 s) was obtained from the fixation phase (Fig. 1c), which also served as the baseline for ERSP calculation. In the end, we obtained 105.25 ± 13.57, 105.08 ± 12.08, and 106.67 ± 11.94 segments for IM, PM, and IPM, respectively. The resting state contained the same number of segments as IM, PM, and IPM, respectively.

The FgMDM classifier was implemented using the Covariance toolbox[2] with the Riemannian mean and distance as model parameters. All models were trained and tested following a 10×5-fold (stratified) cross-validation procedure. The average accuracy (correct predictions out of all samples) is reported.

F. Statistical analysis

We compared the alpha and beta rhythm power changes at channels C3 and C4 via the Wilcoxon rank sum test. We used repeated measures Analysis of Variance (ANOVA) to test the difference of alpha and beta rhythm for different modalities. Once a significant effect was found, we performed multiple comparisons with Bonferroni correction. The classification accuracies from different models were tested in the same way. The normality of variable observations was examined based on the Shapiro-Wilk test. All statistical analyses used a significant level of 0.05.

III. RESULTS

A. Exoskeleton-assisted finger movements induce strong EEG desynchronization in sensorimotor area

Figure 2 illustrates the evolution of EEG activities within the alpha and beta bands for three movement modalities. Each topoplot represents the averaged ERSP across all finger tasks, subjects, and the selected time window. During the preparation stage, IM and IPM exhibited relatively stronger power decreases (i.e., desynchronization or ERD) compared to PM in the contralateral central region, with IPM showing more widespread activation. Upon exoskeleton activation, stronger ERD occurred in the sensorimotor area, as observed in PM and IPM modalities during the task and rest stages. The proprioceptive feedback-induced ERD was bilaterally distributed, with the strongest effects observed contralaterally. It is worth noting that for PM and IPM in the rest stage, the exoskeleton is

---

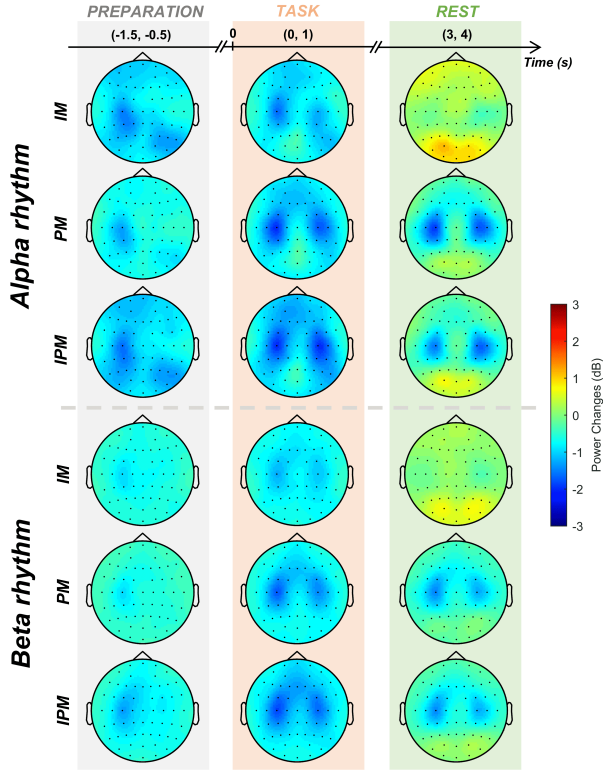[2]https://github.com/alexandrebarachant/covariancetoolbox/tree/master

Fig. 2. Changes in alpha and beta rhythm power distribution over time for different movement modalities across three interaction stages: Preparation, Task, and Rest. Each column represents a distinct stage, with time = 0 s indicating the onset of the task. The color scale shows power changes in dB. EEG electrode locations were marked in black dots.
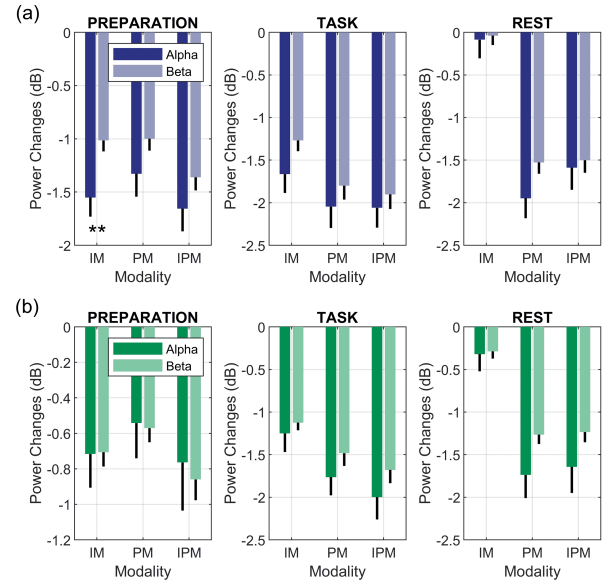

Fig. 3. Comparison between alpha and beta band power changes at channel (a) C3 and (b) C4. From left to right, each subfigure represents a different interaction stage similar to Fig. 2. The whisker on each bar corresponds to the standard error of the mean (SEM) power changes across subjects. The asterisk indicates a significant difference between alpha and beta was found via the Wilcoxon rank sum test (**: $p < 0.01$).

TABLE I
COMPARISON BETWEEN MOVEMENT MODALITIES IN ALPHA AND BETA BAND POWER CHANGES AT CHANNEL C3 AND C4. N.S. INDICATES NOT SIGNIFICANT

Channel	Rhythm	Comparison	P-value
C3	alpha	PM vs. IM	0.00044218
		IPM vs. IM	0.00086206
		IPM vs. PM	n.s.
	beta	PM vs. IM	3.234e-05
		IPM vs. IM	4.5419e-06
		IPM vs. PM	n.s.
C4	alpha	PM vs. IM	0.003176
		IPM vs. IM	5.6824e-05
		IPM vs. PM	n.s.
	beta	PM vs. IM	0.00098239
		IPM vs. IM	9.517e-06
		IPM vs. PM	n.s.

homing back at a faster speed, which partly explains why rest-stage ERD patterns differ from those of the task stage. Additionally, a strong ERS was observed in the occipital region for the IM modality during REST when the subject ceased motor imagery, with a similar but less pronounced effect for IPM and minimal occurrence in PM. For the distribution differences between alpha and beta rhythms, more brain regions engaged in alpha ERD, particularly for the preparation and task stages. The strength of each rhythm at the C3 (contralateral) and C4 (ipsilateral) EEG channel was statistically compared in Fig. 3. Generally, alpha rhythm showed stronger ERD compared to the beta rhythm for the EEG channels of both hemispheres, with the exception of the preparation stage in C4. However, a significant difference between alpha and beta was only found in C3 during the preparation stage of the IM modality (Fig. 3a).

B. Comparable alpha and beta ERD in exoskeleton-assisted movements regardless of motor intentions

Figure 4 presents the time-frequency representation of the C3 and C4 channels for three movement modalities. The 8-30 Hz frequency band activity was most pronounced in each modality, particularly when exoskeleton movement was involved (Fig. 4a and d). During exoskeleton-assisted movement (PM and IPM), stronger ERD was observed compared to

IM. A pronounced ERS was observed in the IM condition after the end of the task, whereas the exoskeleton-induced ERD persisted because of the device homing back. During the task, alpha and beta rhythms showed distinct behaviors, as illustrated in Fig. 4b-c and e-f. Notably, a steep decrease in alpha power was observed upon exoskeleton activation (Fig. 4b and e). In terms of modality differences, PM and IPM showed similar alpha and beta band desynchronization, with minimal variation during the pre- and post-task stages. Table I compares power changes across modalities in the alpha and beta bands during the task stage (time window: 5 - 6s), revealing significant differences for both PM and IPM compared to IM, while no significant difference was detected between PM and IPM.
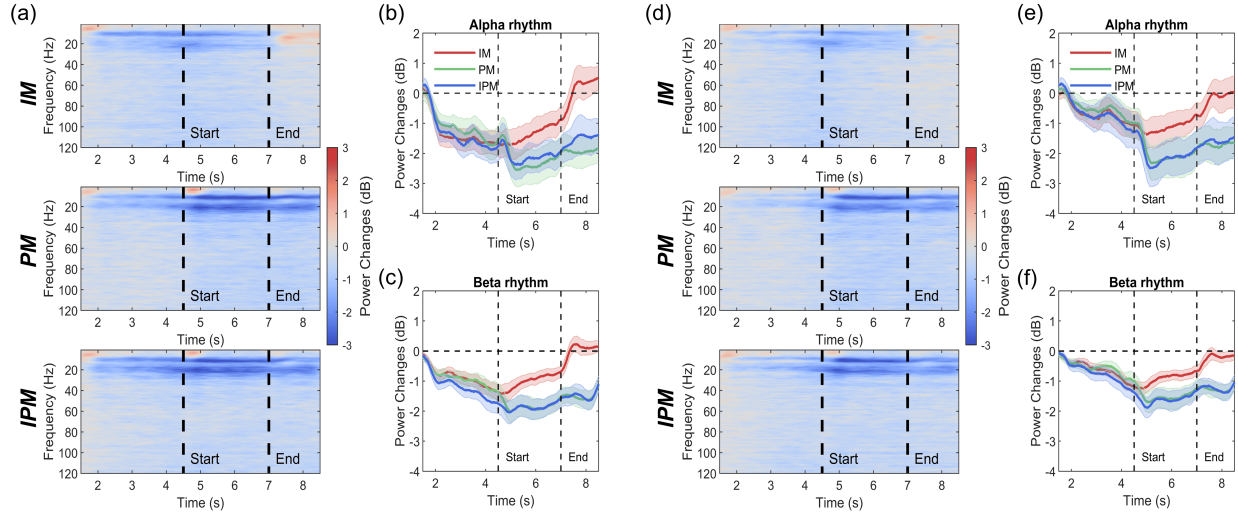
Fig. 4. Time-frequency representation of EEG activity in the C3 (a-c) and C4 (d-f) channels for different movement modalities. (a, d) Time-frequency spectra for IM, PM, and IPM modalities, illustrating power changes in dB over time. (b-c, e-f) Comparison of alpha (8-13 Hz) and beta (13-30 Hz) band power changes across movement modalities. 'Start' and 'End' denote the onset and offset of the task, respectively. Thick lines in (b-c) and (e-f) correspond to the average across trials, shaded regions to the 95% confidence interval.

C. Motor intention detection is more challenging with proprioceptive feedback

Figure 5 presents the binary classification results from four models. In general, distinguishing different movement modalities from the resting state is relatively easy, with the highest accuracy achieved 0.80 ± 0.07 (IPM vs. REST). The worst condition was IPM vs. PM, which obtained an accuracy of 0.61 ± 0.09, thus slightly above the chance level. It is interesting that the models IM vs. REST and PM vs. REST showed no significant difference, and a larger accuracy variation was found for PM vs. REST.

IV. DISCUSSION

As growing attention is being dedicated to BCI-controlled hand exoskeletons, the challenges for advancing this BCI application should be addressed. In this study, we focused on a critical component, namely, motor intention decoding from brain activities during human-hand exoskeleton interaction. From continuous EEG recordings, we observed that exoskeleton-assisted passive movement introduced prominent bilateral ERD in alpha and beta bands, which is similar in frequency range but stronger in amplitude compared to imagined movement-induced neural correlates (Fig. 2 and Fig. 4). When the exoskeleton's movement was involved, it became difficult to discern motor intention-related EEG responses, as reflected by the statistical comparisons between PM and IPM modalities (Table I). This could partially explain why motor intention detection was quite difficult for IPM vs. PM (Fig. 5).

It is worth noting that our study focused specifically on the interaction between humans and a cable-driven hand exoskeleton. EEG correlates may vary across different exoskeleton systems. Our findings align with those reported in [6], where the same hand exoskeleton model was used,
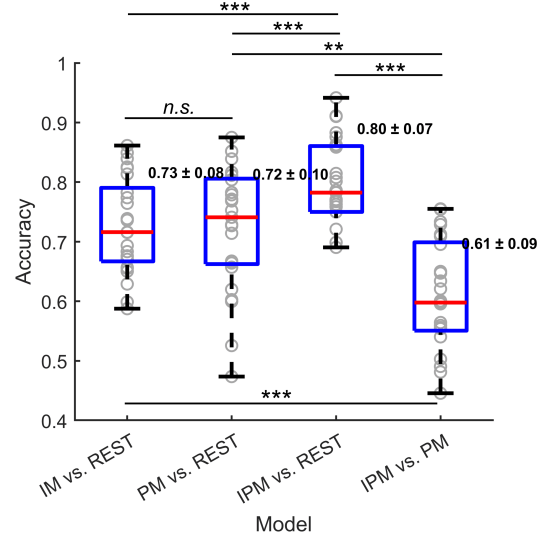

Fig. 5. Comparison between different binary classification models. Each box shows the distribution of each subject's accuracy (n = 25), with the middle red line representing the median. The whiskers correspond to 1.5 × IQR. The average accuracy and standard deviation are shown next to each box. P-values from post-hoc multiple comparisons are marked on the figure (***: $p < 0.001$, **: $p < 0.01$, n.s.: not significant)

and ERD patterns were observed in similar frequency ranges. Although the proprioceptive representation of the hand differs from that of proximal limb counterparts [15], similarities in EEG correlates are evident across the hand (our study and [6]), wrist [5], forearm [16], and lower limb [7]. Generally, passive movement elicits bilateral alpha and beta ERD, with a predominance on the contralateral side. On the other hand, factors such as movement speed and the type of exoskeleton motor will also impact EEG correlates. For example, Iwane

et al. reported that passive movement speed was correlated with the contralateral beta rebound and ipsilateral alpha ERD [16]. Mitra *et al.* observed a strong broadband synchronization coinciding with the robot movement [17], suggesting some exoskeletons (Harmony Exoskeleton used in their study) will likely introduce instrumental noise.

When comparing alpha and beta ERD, we found alpha rhythm had stronger desynchronization than beta rhythm (Fig. 3), particularly on the contralateral side, which is in line with observations in [5], [7], [18]. This supports earlier observations that alpha and beta rhythms would be related to different functional properties, i.e. somatosensory- and somatomotor cortical function, respectively [19]. Another finding in our study is that passive movement produced clear-cut modification of alpha band oscillations compared to beta band upon exoskeleton activation, as depicted in Fig. 4b-c. This could be partially explained by the sensitivity of alpha rhythm to attention and cognitive engagement [20]. During exoskeleton-assisted movements, the subject might pay more attention to the sensation of movement or the mechanical action of the exoskeleton.

We found a significant difference in motor intention detection with and without exoskeleton movement in Fig. 5. With exoskeleton movement, intention detection becomes more challenging (IPM vs. PM compared to IM vs. REST). This phenomenon was also reflected in Ferrero *et al.*'s study [10], where the authors found that it was more challenging to detect 'stop' intention when the lower-limb exoskeleton was activated compared to detecting 'start' intention without robot activation. Our experiment revealed that when the exoskeleton is activated, brain activations are similar regardless of whether the subject imagines a movement (IPM modality) or not (PM modality). In contrast, when the exoskeleton is not involved, the ERD induced by motor imagery (IM modality) can be clearly distinguished from REST. Therefore, extracting motor intention-related EEG features becomes more challenging in situations with exoskeleton activation. An interesting finding is that although both IPM and PM showed significantly different power changes compared to IM (Table I), PM vs. REST did not show as high accuracy as IPM vs. REST, nor IM vs. REST. One explanation is that we were classifying the covariance feature on the manifold space, not the power feature.

Although BCI-actuated hand exoskeletons hold great promise for neurorehabilitation, their current control strategies remain limited. Typically, a BCI decoder detects the user's motor intention and triggers the exoskeleton accordingly. However, once the exoskeleton is activated, the decoder struggles to function effectively, restricting the system to discrete control [21]. This means users can initiate movement but cannot continuously modulate or stop it. A key challenge for the next generation of BCI-exoskeleton systems is enabling continuous control, where motor intentions are dynamically monitored and executed in real-time. Our findings highlight this challenge: during exoskeleton interaction, the brain generates ERD patterns that are similar but stronger than those observed during motor imagery (Fig. 2, Fig. 4). Moreover, our decoding results

suggest that detecting motor intention becomes significantly more difficult when the exoskeleton is moving (IPM vs. PM), with a classification accuracy only marginally above chance level. There is a trade-off between system stability and subject engagement. For stable control and better task completion, one may consider using a shared-control strategy [22] as it relies more on robot intelligence. For natural control and more subject engagement, we believe subject learning and advanced decoders are required. Indeed, although we asked the subject to avoid performing any movement imagination during PM, they reported that it was quite hard to finish the task. This suggested that subject learning is necessary in order to obtain task-differentiable data [23]. Our previous studies have shown the possibility of regressing fine finger movements from intracranial brain activity [24], [25], those explainable models can be particularly useful for continuous motor intention decoding during human-hand exoskeleton interaction.

V. Conclusion

We designed an experiment to investigate the impact of proprioception in EEG representations and decoding when interacting with a hand exoskeleton. We found when the exoskeleton was activated, strong alpha and beta ERDs were elicited due to proprioceptive afferents. However, EEG correlates were similar in situations with and without imagined motor intention upon the exoskeleton activation. Those findings explain why poor motor intention detection accuracy was observed when involving the exoskeleton. For future development of continuous BCI-actuated hand exoskeletons, we suggest using advanced decoders or control strategies considering the trade-off between system stability and subject engagement.

References

[1] J. R. Wolpaw, N. Birbaumer, D. J. McFarland, G. Pfurtscheller, and T. M. Vaughan, "Brain–computer interfaces for communication and control," *Clinical neurophysiology*, vol. 113, no. 6, pp. 767–791, 2002.

[2] S. R. Soekadar, M. Witkowski, C. Gómez, E. Opisso, J. Medina, M. Cortese, M. Cempini, M. C. Carrozza, L. G. Cohen, N. Birbaumer, and N. Vitiello, "Hybrid EEG/EOG-based brain/neural hand exoskeleton restores fully independent daily living activities after quadriplegia," *Science Robotics*, vol. 1, no. 1, p. eaag3296, Dec. 2016.

[3] A. A. Blank, J. A. French, A. U. Pehlivan, and M. K. O'Malley, "Current trends in robot-assisted upper-limb stroke rehabilitation: promoting patient engagement in therapy," *Current physical medicine and rehabilitation reports*, vol. 2, pp. 184–195, 2014.

[4] A. A. Frolov, O. Mokienko, R. Lyukmanov, E. Biryukova, S. Kotov, L. Turbina, G. Nadareyshvily, and Y. Bushkova, "Post-stroke rehabilitation training with a motor-imagery-based brain-computer interface (BCI)-controlled hand exoskeleton: a randomized controlled multicenter trial," *Frontiers in neuroscience*, vol. 11, p. 400, 2017.

[5] E. Formaggio, S. F. Storti, I. Boscolo Galazzo, M. Gandolfi, C. Geroin, N. Smania, L. Spezia, A. Waldner, A. Fiaschi, and P. Manganotti, "Modulation of event-related desynchronization in robot-assisted hand performance: brain oscillatory changes in active, passive and imagined movements," *Journal of NeuroEngineering and Rehabilitation*, vol. 10, no. 1, p. 24, Dec. 2013.

[6] G. Tacchino, M. Gandolla, S. Coelli, R. Barbieri, A. Pedrocchi, and A. M. Bianchi, "EEG analysis during active and assisted repetitive movements: evidence for differences in neural engagement," *IEEE Transactions on Neural Systems and Rehabilitation Engineering*, vol. 25, no. 6, pp. 761–771, Jun. 2017.

[7] E. Formaggio, S. Masiero, A. Bosco, F. Izzi, F. Piccione, and A. Del Felice, "Quantitative EEG evaluation during robot-assisted foot movement," *IEEE Transactions on Neural Systems and Rehabilitation Engineering*, vol. 25, no. 9, pp. 1633–1640, Sep. 2017.

[8] G. Pfurtscheller and F. Lopes Da Silva, "Event-related EEG/MEG synchronization and desynchronization: basic principles," *Clinical Neurophysiology*, vol. 110, no. 11, pp. 1842–1857, Nov. 1999.

[9] F. Cassim, C. Monaca, W. Szurhaj, J. Bourriez, L. Defebvre, P. Derambure, and J. Guieu, "Does post-movement beta synchronization reflect an idling motor cortex?" *Neuroreport*, vol. 12, no. 17, pp. 3859–3863, Dec. 2001.

[10] L. Ferrero, P. Soriano-Segura, J. Navarro, O. Jones, M. Ortiz, E. Iáñez, J. M. Azorín, and J. L. Contreras-Vidal, "Brain–machine interface based on deep learning to control asynchronously a lower-limb robotic exoskeleton: a case-of-study," *Journal of NeuroEngineering and Rehabilitation*, vol. 21, no. 1, p. 48, 2024.

[11] R. Oostenveld, P. Fries, E. Maris, and J.-M. Schoffelen, "FieldTrip: open source software for advanced analysis of MEG, EEG, and invasive electrophysiological data," *Computational Intelligence and Neuroscience*, vol. 2011, no. 1, pp. 1:1–1:9, 2011.

[12] Q. Sun, E. C. Merino, L. Yang, and M. M. Van Hulle, "Unraveling EEG correlates of unimanual finger movements: insights from non-repetitive flexion and extension tasks," *Journal of NeuroEngineering and Rehabilitation*, vol. 21, no. 1, p. 228, 2024.

[13] A. Barachant, S. Bonnet, M. Congedo, and C. Jutten, "Riemannian geometry applied to bci classification," in *International conference on latent variable analysis and signal separation*. Springer, 2010, pp. 629–636.

[14] S. Chevallier, I. Carrara, B. Aristimunha, P. Guetschel, S. Sedlar, B. Lopes, S. Velut, S. Khazem, and T. Moreau, "The largest EEG-based BCI reproducibility study for open science: the MOABB benchmark," *arXiv preprint arXiv:2404.15319*, 2024.

[15] O. J. Lutz and S. J. Bensmaia, "Proprioceptive representations of the hand in somatosensory cortex," *Current Opinion in Physiology*, vol. 21, pp. 9–16, 2021.

[16] F. Iwane, G. Lisi, and J. Morimoto, "EEG sensorimotor correlates of speed during forearm passive movements," *IEEE Transactions on Neural Systems and Rehabilitation Engineering*, vol. 27, no. 9, pp. 1667–1675, Sep. 2019.

[17] K. Mitra, F. S. Racz, S. Kumar, A. D. Deshpande, and J. D. R. Millán, "Characterizing the onset and offset of motor imagery during passive arm movements induced by an upper-body exoskeleton," in *2023 IEEE/RSJ International Conference on Intelligent Robots and Systems (IROS)*. IEEE, 2023, pp. 3789–3794.

[18] E. Formaggio, S. F. Storti, I. Boscolo Galazzo, M. Gandolfi, C. Geroin, N. Smania, A. Fiaschi, and P. Manganotti, "Time–frequency modulation of ERD and EEG coherence in robot-assisted hand performance," *Brain topography*, vol. 28, pp. 352–363, 2015.

[19] A. Stolk, L. Brinkman, M. J. Vansteensel, E. Aarnoutse, F. S. Leijten, C. H. Dijkerman, R. T. Knight, F. P. de Lange, and I. Toni, "Electrocorticographic dissociation of alpha and beta rhythmic activity in the human sensorimotor system," *Elife*, vol. 8, p. e48065, 2019.

[20] J. A. Pineda, "The functional significance of mu rhythms: translating "seeing" and "hearing" into "doing"," *Brain research reviews*, vol. 50, no. 1, pp. 57–68, 2005.

[21] N. Rustamov, L. Souders, L. Sheehan, A. Carter, and E. C. Leuthardt, "IpsiHand brain-computer interface therapy induces broad upper extremity motor recovery in chronic stroke," *medRxiv*, pp. 2023–08, 2023.

[22] J. M. Catalán, E. Trigili, M. Nann, A. Blanco-Ivorra, C. Lauretti, F. Cordella, E. Ivorra, E. Armstrong, S. Crea, M. Alcañiz *et al.*, "Hybrid brain/neural interface and autonomous vision-guided whole-arm exoskeleton control to perform activities of daily living (adls)," *Journal of NeuroEngineering and Rehabilitation*, vol. 20, no. 1, p. 61, 2023.

[23] S. Perdikis, L. Tonin, S. Saeedi, C. Schneider, and J. d. R. Millán, "The Cybathlon BCI race: Successful longitudinal mutual learning with two tetraplegic users," *PLoS biology*, vol. 16, no. 5, p. e2003787, 2018.

[24] A. Faes, F. Camarrone, and M. M. Van Hulle, "Single finger trajectory prediction from intracranial brain activity using block-term tensor regression with fast and automatic component extraction," *IEEE Transactions on Neural Networks and Learning Systems*, 2022.

[25] A. Faes and M. Van Hulle, "Finger movement and coactivation predicted from intracranial brain activity using extended block-term tensor regression," *Journal of Neural Engineering*, vol. 19, no. 6, p. 066011, 2022.